Geophysical Research Letters

RESEARCH LETTER
10.1029/2018GL079103

Special Section:
Initial results of the ERG (Arase) project and multi-point observations in geospace

Purple Auroral Rays and Global Pc1 Pulsations Observed at the CIR-Associated Solar Wind Density Enhancement on 21 March 2017

K. Shiokawa[1], M. Ozaki[2], A. Kadokura[3,4,5], Y. Endo[4,6], T. Sakanoi[4,6], S. Kurita[1], Y. Miyoshi[1], S.-I. Oyama[1,3,7], M. Connors[8], I. Schofield[8], J. M. Ruohoniemi[9], M. Nośe[1], T. Nagatsuma[10], K. Sakaguchi[10], D. G. Baishev[11], A. Pashinin[12], R. Rakhmatulin[12], B. Shevtsov[13], I. Poddelsky[13], M. Engebretson[14], Tero Raita[15], Y.-M. Tanaka[3,4,5], M. Shinohara[16], M. Teramoto[1], R. Nomura[17], A. Fujimoto[18], A. Matsuoka[19], N. Higashio[17], T. Takashima[19], I. Shinohara[19], and Jay M. Albert[20]

[1]Institute for Space-Earth Environmental Research, Nagoya University, Nagoya, Japan, [2]Kanazawa University, Kakuma, Japan, [3]National Institute of Polar Research, Tachikawa, Japan, [4]Polar Environment Data Science Center, Joint Support-Center for Data Science Research Research Organization of Information and Systems, Japan, [5]The Graduate University for Advanced Studies (SOKENDAI), Japan, [6]Graduate School of Science, Tohoku University, Aoba-ku, Japan, [7]University of Oulu, Oulu, Finland, [8]Observatories, Athabasca University, Athabasca, Alberta, Canada, [9]Bradley Department of Computer and Electrical Engineering, Space@VT, Virginia Tech, Blacksburg, VA, USA, [10]National Institute of Information and Communications Technology, Koganei, Japan, [11]Yu.G.Shafer Institute of Cosmophysical Research and Aeronomy, Siberian Branch of the Russian Academy of Sciences, Yakutsk, Russia, [12]Institute of Solar-Terrestrial Physics, Siberian Branch of the Russian Academy of Sciences, Irkutsk, Russia, [13]Institute of Cosmophysical Researches and Radio Wave Propagation (IKIR), Far Eastern Branch of the Russian Academy of Sciences, Paratunka, Russia, [14]Department of Physics, Augsburg University, Minneapolis, MN, USA, [15]Sodankylä Geophysical Observatory, University of Oulu, Sodankylä, Finland, [16]National Institute of Technology, Kagoshima College, Kirishima, Japan, [17]Japan Aerospace Exploration Agency, Tsukuba-shi, Japan, [18]Kyushu Institute of Technology, Iizuka, Japan, [19]Institute of Space and Astronautical Science, Japan Aerospace Exploration Agency, Sagamihara, Japan, [20]Air Force Research Lab/RVBXA, Kirtland, OH, USA

Key Points:
- Unique postmidnight purple auroral rays and global Pc1/EMIC waves were observed during a CIR-driven solar wind density enhancement
- Pc1/EMIC waves were found over a wide longitudinal range extending from midnight through morning to the afternoon due to CIR arrival
- Entry of high-density solar wind plasma into the magnetotail may have created tall purple auroral rays in the sunlit ionosphere

Supporting Information:
- Supporting Information S1
- Movie S1
- Movie S2

Correspondence to:
K. Shiokawa,
shiokawa@nagoya-u.jp

Citation:
Shiokawa, K., Ozaki, M., Kadokura, A., Endo, Y., Sakanoi, T., Kurita, S., et al. (2018). Purple auroral rays and global Pc1 pulsations observed at the CIR-associated solar wind density enhancement on 21 March 2017. *Geophysical Research Letters*, *45*, 10,819–10,828. https://doi.org/10.1029/2018GL079103

Received 10 JUN 2018
Accepted 26 SEP 2018
Accepted article online 1 OCT 2018
Published online 18 OCT 2018

©2018. American Geophysical Union. All Rights Reserved.

Abstract This paper reports two unique auroral features: postmidnight purple auroral rays and global Pc1 geomagnetic pulsations, observed before the onset of the corotating interaction region (CIR) storm of 21 March 2017, at the beginning of the first campaign of the new Particles and Waves in the Inner magnetosphere using Ground-based network observation (PWING) longitudinal ground network with the Arase satellite. The purple auroral rays were observed from ~0315 to 0430 UT (~03–04 magnetic local time) in the northeastern sky at Husafell, Iceland (magnetic latitude: 64.9°N). We newly propose that the entry of high-density CIR plasma into the magnetotail created purple auroral rays in the sunlit ionosphere. Pc1 geomagnetic pulsations at frequencies of 0–0.5 Hz were observed after ~00 UT over a wide local time range, of 13 hr, from midnight to afternoon sectors at subauroral latitudes associated with CIR arrival. These results indicate preconditioning of the magnetosphere due to crossing of a CIR.

Plain Language Summary We report auroral ray structures, which show a unique purple color, and global geomagnetic pulsations observed on 17 March 2017. The purple auroral rays were observed in the northeastern sky at Husafell, Iceland. The geomagnetic pulsations at frequencies of below 0.5 Hz were observed over a wide longitudinal range extending from midnight through morning to afternoon sectors at subauroral latitudes. These phenomena took place associated with the arrival of the so-called corotating interaction region (CIR)" in the interplanetary space, which is characterized by high-density high-speed solar wind plasma. The CIR is one of the phenomena frequently occurring during the minimum phase of the 11-year solar cycle. We suggest that the CIR can cause these unique purple auroras and global geomagnetic pulsations. The present observations also suggest a possible mechanism for dropout of radiation belt electrons due to electromagnetic ion cyclotron waves (=geomagnetic pulsations) associated with the CIR arrival.

1. Introduction

Corotating interaction regions (CIRs) are caused by high-speed solar winds emanating from solar coronal holes that interact with upstream slow solar winds (e.g., Tsurutani et al., 2006). CIRs are among the major structures in the solar wind that can cause geomagnetic storms in the absence of solar eruptive events,

such as coronal mass ejections (CMEs), particularly during solar quiet times. There have been several studies of the differences between geomagnetic storms associated with CMEs and CIRs (e.g., Borovsky & Denton, 2006; Fraser et al., 2010; Kataoka & Miyoshi, 2006; Miyoshi & Kataoka, 2005; Sandanger et al., 2009; Tsurutani et al., 1995; Zhou & Smith, 2015). CIR storms tend to be weaker than CME storms in terms of ring current intensities as indicated by the Dst index. CIR storms may generate radiation belt particles more effectively due to their longer durations and fluctuating interplanetary magnetic field (IMF), resulting in hazardous conditions for spacecraft (e.g., Iles et al., 2002; Miyoshi et al., 2013; Miyoshi & Kataoka, 2008; Tsurutani, 2001).

On the arrival of a CIR, solar wind monitoring satellites at 1 AU typically observe an enhancement in the solar wind plasma density, followed by an increase in the solar wind speed and development of a turbulent IMF containing a southward IMF-Bz, which initiates the main phase of a geomagnetic storm. Because the time period prior to the CIR storm is characterized by enhanced solar wind density, there might be unique effects in the Earth's magnetosphere associated with the injection of high-density plasma into the magnetotail region before the start of the main phase of the storm (i.e., preconditioning), as pointed out by Borovsky and Denton (2006). Auroral features at the beginning of the CIR storm may reflect the effect of this preconditioning, although these features have not been well studied to date. This preconditioning and subsequent increase in solar wind speed and IMF fluctuations may also contribute to the generation of various waves by setting up unstable plasma conditions in the magnetosphere.

The first observational campaign of the inner magnetosphere by the Arase satellite (and ground observation networks) was held from 20 March to 30 April 2017. A new longitudinal ground network covering all local times at subauroral latitudes became available through the "Study of dynamical variation of Particles and Waves in the Inner magnetosphere using Ground-based network observations (PWING)" project. In this paper, we used data from the first campaign observation and report two unique features: postmidnight tall purple auroral rays and global Pc1 geomagnetic pulsations, observed just before the beginning of the CIR storm of 21 March 2017. The tall purple auroral rays in the postmidnight sector suggest the entry of high-density solar wind plasma into the magnetotail flank. The unique PWING longitudinal network makes it possible to identify Pc1 pulsations occurring over a wide longitudinal range extending from midnight to the afternoon sector that are associated with the arrival of high-density solar wind plasma, even though the CIR storm had not yet begun. These Pc1 pulsations, specifically electromagnetic ion cyclotron (EMIC) waves in the magnetosphere (e.g., Fujita & Tamao, 1988; Greifinger, 1972), may contribute to the scattering loss of radiation belt particles in the inner magnetosphere to the ionosphere through wave-particle interactions.

2. Observation

Since April 2016, the PWING project has deployed all-sky imagers, induction magnetometers, riometers, and very low frequency receivers at eight stations at subauroral latitudes of ~60°N magnetic latitude (MLAT) around the north geomagnetic pole, to identify the longitudinal distribution of waves and particle precipitation arising from the inner magnetosphere (Shiokawa et al., 2017). The Arase (ERG) satellite was launched on 20 December 2016 and has been in full operation since March 2017(Miyoshi et al., 2018). Thus, the first Arase-ground campaign observation of the inner magnetosphere was held from 20 March to 30 April 2017. The combination of these ground and satellite instruments provides a unique opportunity to measure longitudinal distribution of various types of waves together with the in situ measurements of radiation belt electrons.

Figures 1a–1h show the three-component IMF, solar wind speed, density, temperature, AU and AL indices, and SYM-H index obtained from the OMNI database of National Aeronautics and Space Administration (NASA) for 20 and 21 March 2017 at the beginning of the campaign. The solar wind density started to increase from ~23 UT on 20 March from 10 to 50/cm^3 at ~0530 UT on 21 March (Figure 1e). The increase in solar wind speed was less significant during this interval. Solar wind density enhancement is a typical feature of the CIR prior to the arrival of high-speed solar wind, indicating the compression of plasmas in front of the high-speed stream (e.g., Tsurutani et al., 2006). Solar wind speed (Figure 1d) increased significantly from ~300 km/s to more than 600 km/s after 15 UT, with increasing proton temperature in Figure 1f from 07 UT, indicating the arrival of the high-speed solar wind. The IMF Bz (Figure 1c) remained northward until ~0320 UT, before turning southward from 0320 UT, and then again more significantly from 0630 UT; after 13 UT, the CIR storm developed, as shown by the SYM-H index (Figure 1h). At the beginning of the CIR storm, a small substorm

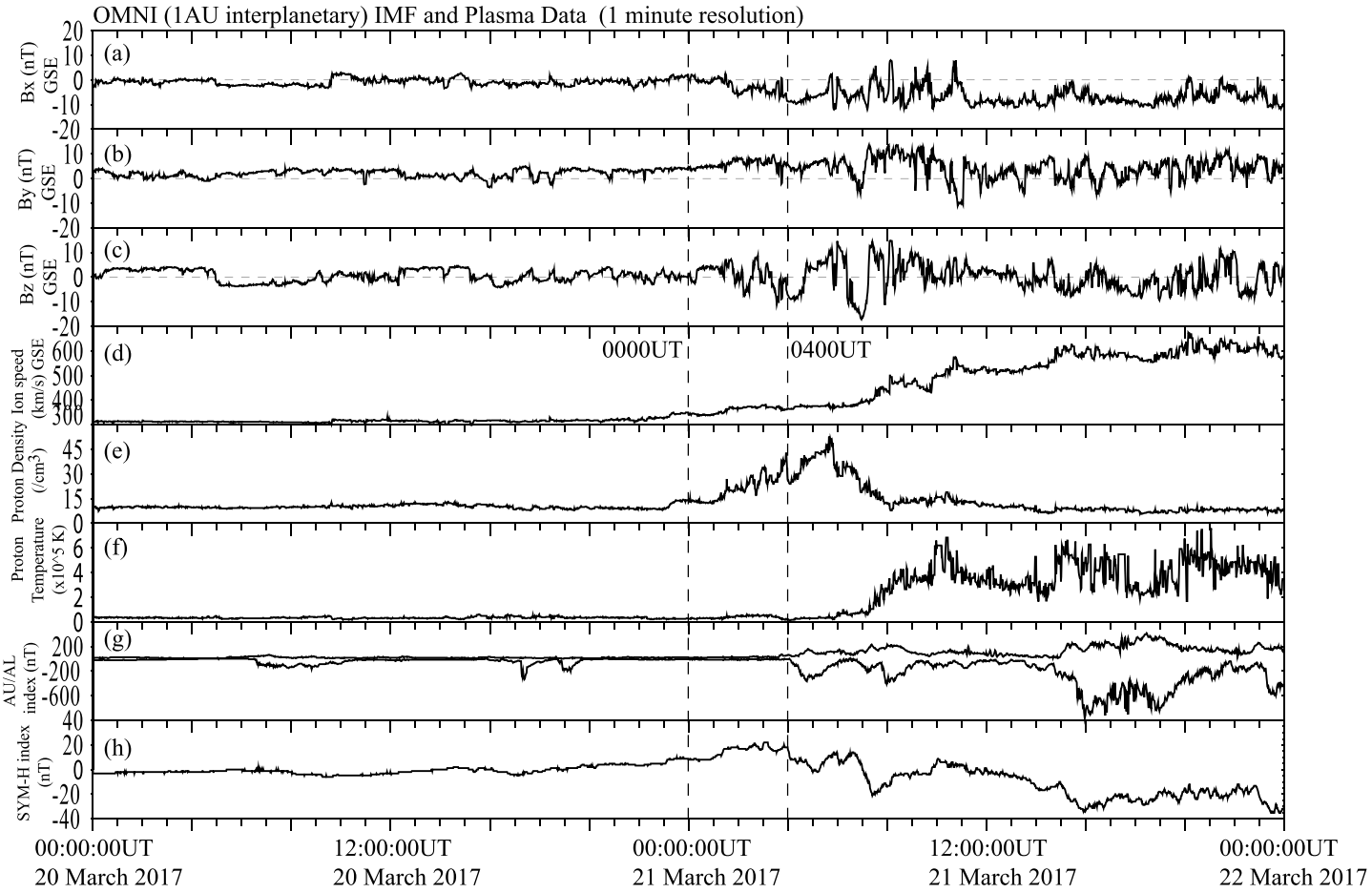

Figure 1. (a–c) Three components of the interplanetary magnetic field (IMF), (d) solar wind speed, (e) density, (f) temperature, (g) AU and AL indices, and (h) SYM-H index obtained from the OMNI database over 2 days (20–21 March 2017).

took place from 0400 UT, with a minimum AL index of ~300 nT, associated with the initial southward turning of IMF Bz.

Figure 2 shows sequential auroral images taken by a Nikon D40 digital camera (ISO1600), with a 35 mm/F1.4 lens and an exposure time of 15 s, of the northeastern sky at Husafell (HUS, 64.67°N, 338.97°E, MLAT: 64.9°N), Iceland, at 0315–0432 UT on 21 March 2017. The complete set of images from 0308 to 0432 UT is shown in Movie S1. These images were taken manually through a window by an observer (K. S.) who stayed at HUS for the campaign observation. Notably, room light contaminated the images several times (e.g., at 0308, 0311, and 0340–0341 UT).

Clear purple auroral rays are visible in the images of Figure 2 and Movie S1 from 0308 to 0432 UT. Because no images were taken before 0308 UT, we do not know when these purple rays appeared initially. In Movie S1, the purple auroral rays showed repeated eastward (sunward) motion. The rays were brightest and most active from 0405 to 0420 UT. It is noticeable that the purple emission was observed mostly in the upper part of the auroral rays.

A stable green east-west auroral arc can also be seen with the purple auroral rays. The green arc gradually moved southward. After 0432 UT, the green aurora transformed into active diffuse auroras with pulsating patches covering the entire sky of HUS; this phenomenon was associated with the onset of a small substorm at 0400 UT (03:40 MLT at HUS).

Movie S2 shows all-sky auroral images at HUS taken by a panchromatic charge-coupled device camera (WAT-120 N+; Watec) with a fish-eye lens (YV2.2X1.4A; Fujinon) from 0000 to 0532 UT on 21 March 2017. The top and left of the images correspond to the north and east directions, respectively. We could not identify the

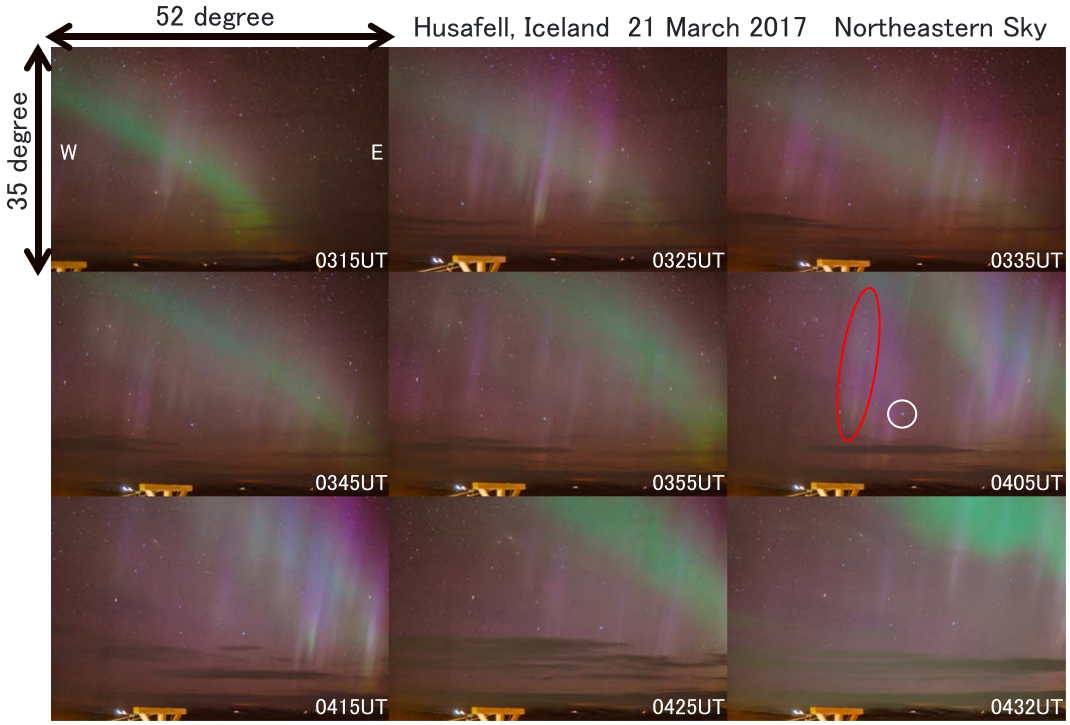

Figure 2. Sequential auroral images taken by a Nikon D40 digital camera with a 35 mm/F1.4 lens and an exposure time of 15 s in the northeastern sky at Husafell (HUS), Iceland, at 0315–0432 UT on 21 March 2017. The star marked by the white circle in the 0405 UT image is Alpheratz.

purple auroral rays in these images. This is probably because usually panchromatic charge-coupled device detectors have higher sensitivities at red to near-infrared wavelengths and less sensitive to the blue to ultraviolet wavelength. So it is natural that this auroral camera is less sensitive to the purple aurora. However, spatiotemporal development of the stable green arc was clearly evident in the images. The arc appeared gradually in the northern sky of HUS at ~01 UT and remained there until 0340 UT, after which it moved slowly toward the equator from 0340 to 0400 UT. After 0420 UT, the arc brightened several times from west to east, and finally converted into active diffuse auroras after 0430 UT, drifting eastward continuously.

Figure 3 shows the dynamic spectra of *H*-component magnetic field variations observed by induction magnetometers at the PWING stations from 1200 UT on 20 March to 1200 UT on 21 March 2017. These spectra were calculated using an ordinary fast Fourier transforms every 128 s (8,192 data points). The magnetic local midnight is shown by a vertical black line in of each panel. The locations of these stations and their full names are shown in the MLT-MLAT map in Figure 4a. At 0020 UT, HUS is at magnetic midnight. The stations in Figures 3d–3f (IVA, IST, ZGN, GAK, ATH, KAP, NAI, and HUS) are longitudinally separated around the north geomagnetic pole at 60–65° MLAT, while those in Figures 3a–3c (MOS and MGD) are midlatitude stations in the longitude of ZGN. These spectra are shown in units of nT^2/Hz, with induction magnetometer sensitivities similar to those cited by Shiokawa et al. (2010, 2017), except for HUS, for which raw voltage data were used due to a lack of calibration data. The magnetometers at Nain are a part of the MACCS (Magnetometer Array for Cusp and Cleft Studies) array (Engebretson et al., 1995), with a sampling rate of 2 Hz.

From 0100 to 0330 UT on 21 March, clear Pc1 geomagnetic pulsations at frequencies of 0–0.5 Hz were observed simultaneously at all of the stations shown in Figure 3, with the exception of NAI, ATH, and KAP. This time interval corresponds to the time when the solar wind density enhancement became significant in Figure 1, while the IMF was still northward and no substorm/storm had developed in the magnetosphere. The stations that observed this simultaneous Pc1 pulsation are denoted by black circles in Figure 4a. These stations are distributed over a wide longitudinal range extending from midnight (HUS), through morning (IVA, IST, and ZGN), to the afternoon (GAK) sector. Pc1 pulsations were not observed in the evening sector

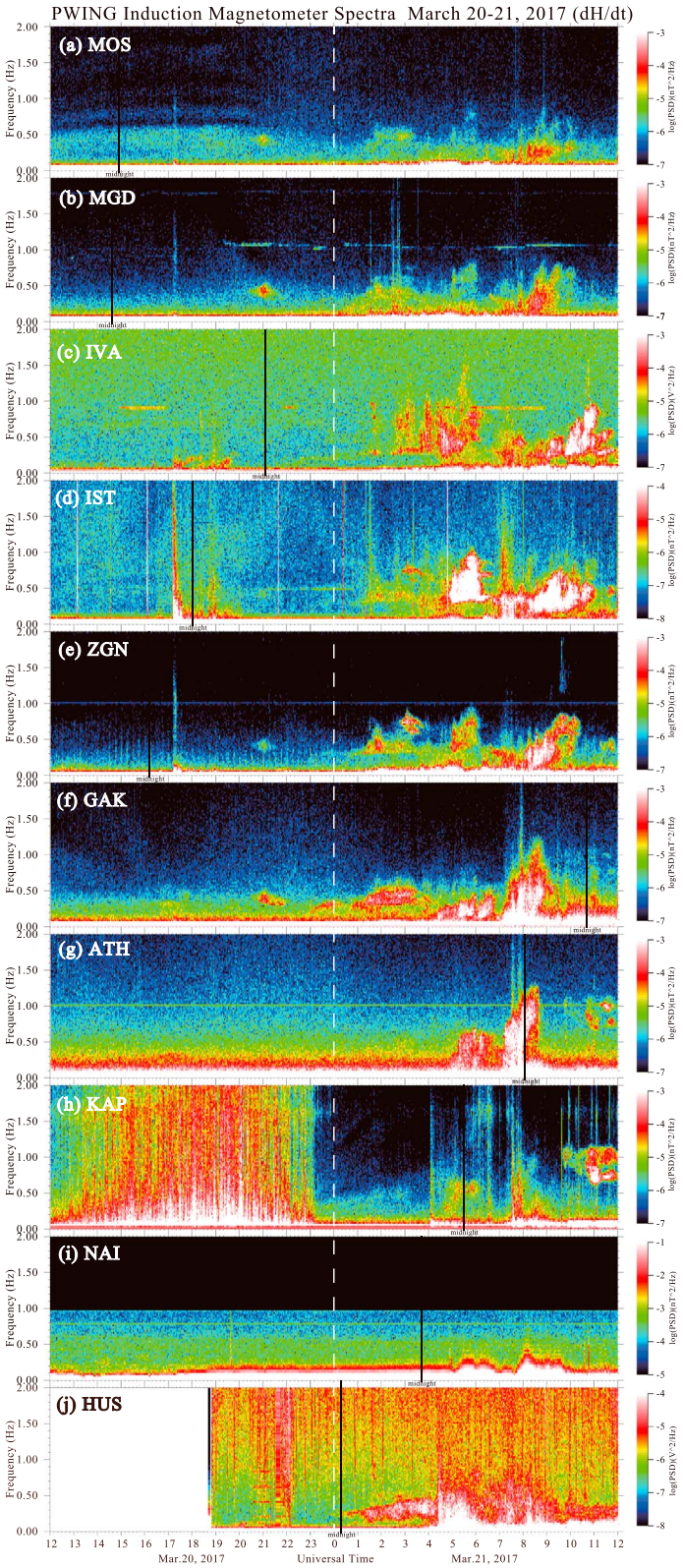

Figure 3. Dynamic spectra of *H*-component magnetic field variations observed by induction magnetometers at the PWING stations from 1200 UT on 20 March to 1200 UT on 21 March 2017. The vertical white dashed line indicates 0000 UT on 21 March. Magnetic local midnight is shown by a vertical black line in each panel. Spectra from HUS and IVA are expressed in units of V^2/Hz, while the other stations used nT^2/Hz.

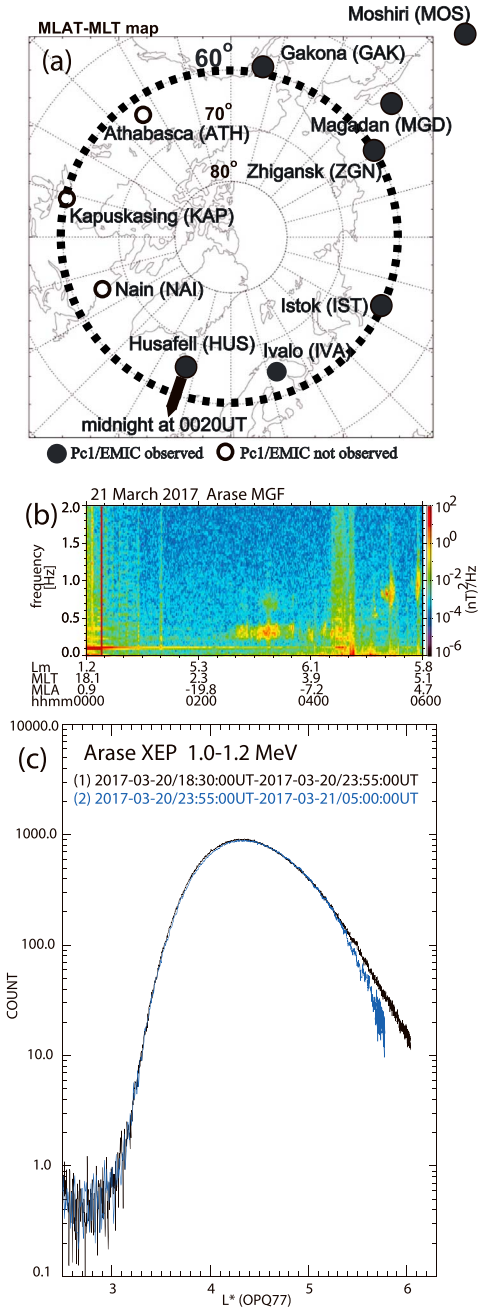

Figure 4. (a) PWING station locations (and their full names) where the induction magnetometer measurements were carried out to obtain the dynamic spectra shown in Figure 3. The black and white circles indicate the stations where Pc1/electromagnetic ion cyclotron (EMIC) waves were observed and not observed, respectively, from 0100 to 0330 UT on 21 March 2017. (b) Dynamic spectra of magnetic field variations obtained by the fluxgate magnetometer onboard the Arase satellite near the conjugate point of HUS. The spectra correspond to the 64-Hz-sampled *z*-component magnetic field in DSI coordinates. Pc1 pulsations/EMIC waves were observed at frequencies of ~0.2–0.4 Hz at ~0220–0340 UT and over a wider frequency range up to ~1 Hz after 0400 UT. (b) Comparison of the high-energy electron fluxes in the radiation belts measured by the extremely high-energy electron experiments (XEP) onboard the Arase satellite for two sequential paths: (1) 1830–2355 UT on 20 March (before the EMIC waves/storm) and (2) from 2355 UT on 20 March to 0500 UT on 21 March (with EMIC waves).

(ATH, KAP, and NAI). The first signature of Pc1 pulsations was detected at GAK dayside at ~2240 UT on 20 March. Another Pc1 pulsation burst occurred at 2050–2120 UT, localized at the dayside stations of GAK and ZGN and midlatitude stations (MGD an MOS) at ~0.3–0.5 Hz. After 0400 UT 21 March, strong Pc1 pulsations with a signature of intervals of pulsations of diminishing periods were observed globally at most of the stations associated with substorm/storm activity.

During the Pc1 pulsation event, the footprint of the Arase satellite was close to HUS. The footprint moved from ~500 km south of HUS at 01 UT (Arase at L~3; here, L is the Roeder L-value from the [International Geomagnetic Reference Field] IGRF and the Olson–Pfitzer Quiet model [OPQ77]; Olson & Pfitzer, 1977), then northeastward within ~700 km east of HUS at 02–04 UT (Arase at L ~ 5–6 and 2–4 MLT), and finally westward approaching within 100 km of HUS at 05 UT (L ~ 6 and ~4.5 MLT). The fluxgate magnetometer onboard the Arase satellite (Matsuoka et al., 2018) observed similar Pc1 pulsations (EMIC waves in the inner magnetosphere) at frequencies of ~0.2–0.4 Hz at ~0220–0340 UT, and over a wider frequency range up to ~1 Hz after 0400 UT, as shown in Figure 4b in the spectra of the *z*-component magnetic field in Despun Sun sector Inertia coordinate (DSI). The DSI-*z* component is the direction of the satellite spin axis, which is basically toward the Sun (GSM-X direction), with a deviation of 10 ± 5°. This Arase observation also confirmed the existence of Pc1 pulsations/EMIC waves in the inner magnetosphere at L ~ 5–6, at the beginning of the CIR storm.

3. Discussion

Purple auroras have been categorized as auroral color class *f* (blue- or purple-dominant) by the International Auroral Atlas (International Union of Geodesy and Geophysics [IUGG], 1963). The IUGG (1963) described the color class f aurora as follows: "Blue colour arises mainly from the ionized nitrogen bands and is commonly dominant during or after very active displays. Mixture with the red atomic oxygen lines gives the appearance of purple. Blue or purple is frequently more noticeable in the upper regions of the aurora and is enhanced when the upper regions are sunlit."

The characteristics of the present purple auroral rays shown in Figure 2 are fairly consistent with the above description of color class f of IUGG (1963), because they were observed dominantly in the upper regions of the aurora. We also checked whether the auroral region was sunlit or not using the star Alpheratz, marked by the white circle in the 0405 UT image in Figure 2. Alpheratz was at an elevation of 12.163° and an azimuth of 224.790° at this time. The auroral ray marked by the red circle in Figure 2 shows green (557.7 nm) emission at the bottom at the same elevation angle as Alpheratz. If we assume that this green auroral bottom edge near this star was at an altitude of 110 km, the geographic location of the aurora becomes (67.28°N, 13.19°W), giving the shadow height of the sunlight at this location at 0405 UT to be 350 km. If we change the assumption of the bottom edge height of the aurora from 110 km to 150 and 170 km, the shadow height changes to 300 and 280 km, respectively. So we can say that the ionosphere above ~280–350 km was sunlit at this time. A simple geometric calculation shows the consistency of the present event with the statement of the IUGG (1963) that the blue or purple aurora is enhanced when the upper region is sunlit. Several previous studies after

that of the IUGG (1963) confirmed that the blue emission, mainly from N_2^+(1NG) at a wavelength of 427.8 nm, comes from the sunlit auroral region through resonant scattering of sunlight by N_2^+ ions produced by auroral ionization (e.g., Hunten, 2003, and references therein). Because this auroral emission was observed at higher altitudes, the N_2^+ ions may have been transported upward from their site of production at lower altitudes.

An interesting difference between the present event and that described by the IUGG (1963) is that the present event was observed during relatively quiet auroras, before the start of the first substorm (0400 UT) of the CIR storm. In particular, the present purple auroral rays at 0308–0432 UT on 21 March were observed during the period of solar wind density enhancement that began 23 UT on 20 March, with prolonged (~7 hr) northward IMF from ~20 UT on 20 March associated with CIR arrival, as shown in Figure 1. Terasawa et al. (1997) pointed out, based on statistical analysis of GEOTAIL satellite data, that during prolonged northward IMF periods (approximately several hours), solar wind plasma is transported diffusively to the near-Earth plasma sheet through the magnetotail flanks, forming the cold dense plasma sheet. The high correlation of plasma densities in the solar wind and plasma sheet was also shown by Borovsky et al. (1998). Thus, the high density solar wind with prolonged northward IMF seen for the present event most likely caused an increase in the cold plasma density in the near-Earth plasma sheet. Borovsky and Steinberg (2006) showed that "a calm before the storm," typically seen just before CIR-storm onset, enhances the contribution to the inner plasma sheet and ring current by the convection of cool dense plasma into the dipole field. This may also contribute to the creation of purple auroral rays through low-energy large-flux electron precipitation in the postmidnight sunlit ionosphere. The repeated eastward (sunward) motion of the purple auroral rays also suggests that the source of this aurora exists in the sunward convecting near-Earth plasma sheet, rather than the antisunward convecting solar wind or low-latitude boundary layer.

The other interesting feature associated with solar wind density enhancement during CIR arrival is the Pc1 pulsations/EMIC waves observed over a wide longitudinal range from midnight to the afternoon sectors. The unique PWING stations enable Pc1/EMIC observation at subauroral latitudes over the entire longitudinal range. Engebretson et al. (2015) showed EMIC appearance over 12-hr local times, stimulated by a gradual 4-hr rise and subsequent sharp increase in solar wind pressure on 23 February 2014. The present Pc1/EMIC waves were observed from HUS to GAK over 13 hr of local time. The magnetosphere was probably compressed gradually due to the solar wind density enhancement from ~23 UT on 20 March (~10/cm^3) to ~0530 UT on 21 March (50/cm^3); however, the compression was more gradual than the sudden compression events reported in previous studies (e.g., Engebretson et al., 2002; Engebretson et al., 2015; Kim et al., 2017; Olson & Lee, 1983; Usanova et al., 2008). Park et al. (2016) reported that Pc1/EMIC waves in a geosynchronous orbit can be generated even by small solar wind pressure enhancements under magnetically quiet conditions.

Before this CIR arrival, the magnetosphere was fairly quiet with only some small substorms (minimum AL index of ~300 nT) occurring from 18 to 20 March. The provisional Dst index was within ±5 nT from 18 to 20 March, except for a reading of +9 nT at 23 UT on 20 March. Thus, we would not expect there to be a sufficient number of high-energy ions to create EMIC waves in the inner magnetosphere. The entry of high-density solar wind plasma into the near-Earth plasma sheet under the northward IMF condition, and the compression of the magnetosphere due to the solar wind density enhancement, may create another population of high-energy ions in the plasma sheet through betatron acceleration. Subsequent generation of EMIC waves may occur through temperature anisotropy due to perpendicular ion acceleration through the betatron process in the conservation of the first adiabatic invariant (e.g., Arnoldy et al., 2005). The Pc1/EMIC waves of the present event were observed from midnight to the morning and dayside sectors. This fact is opposite to the duskward drift of ions injected from the nightside plasma sheet and may suggest betatron acceleration of ions due to dayside magnetospheric compression. The perpendicular betatron acceleration of preexisting ring current ions may generate EMIC waves in the equatorial plane of the magnetosphere. Engebretson et al. (2015) also reported dayside-morningside enhancement of EMIC waves associated with an increase in solar wind pressure.

These Pc1/EMIC waves may contribute to the loss of radiation belt electrons in the inner magnetosphere through wave-particle interactions, as suggested in the literature (e.g., Hyun et al., 2014; Jordanova et al., 2008; Omura & Zhao, 2012; Summers & Thorne, 2003). We compared the high-energy (1.0–1.2 MeV) electron fluxes in the radiation belts measured by the extremely high-energy electron experiments (XEP; Higashio et al., 2018) onboard the Arase satellite for four sequential paths (1) at 1830–2355 UT on 20 March (before the EMIC

waves/storm) and (2) from 2355 UT on 20 March to 0500 UT on 21 March (during the presence of EMIC waves; Figure 4c). The fluxes in paths (1) and (2) did not differ much. Thus, the global Pc1/EMIC waves at 0100–0330 UT on 21 March may not appear to have contributed to the loss of radiation belt electrons, except for the decrease between (1) and (2) at $L > 5.3$, although the waves were observed over a wide longitudinal range.

We also estimated the loss lifetimes of high-energy electrons by the observed Pc1/EMIC waves based on the method and ion composition ratio described by Miyoshi et al. (2008). The background plasma density observed by Arase at 0100–0400 UT at L = 5–6 in the postmidnight sector near the conjugate point of HUS was relatively high at 100–200/cm^3 as measured by the Plasma Wave Experiment/High Frequency Analyzer (PWE/HFA) instrument (Kumamoto et al., 2018). Arase was on an outbound path and was inside the plasmapause until ~04:40UT (L = 6.2) when the substorm caused a sudden density decrease at the satellite location. During this event, the plasmasphere seems to have expanded significantly, probably because of prolonged quiet condition before this event. Assuming a 100/cm^3 plasma density at L = 6 and a wave amplitude of 0.5 nT at 0.2–0.4 Hz as observed by Arase at 0300–0330 UT, the estimated loss lifetimes are 20,708 s (5.8 hr) at 1 MeV and 1,385 s (23 min) at 10 MeV. The duration of EMIC waves at Arase (0300–0330 UT) can be due to the orbital motion of the satellite and the actual duration of EMIC waves can be much longer (~0100–0330 UT as observed at ground stations in Figure 3). Thus, these Pc1/EMIC waves may contribute to the observed loss of radiation belt electrons between (1) and (2) at $L > 5.3$ in Figure 4c.

4. Conclusions

The first observational campaign of the inner magnetosphere by the Arase satellite and the PWING ground observation networks was held from 20 March to 30 April 2017. The new PWING longitudinal network covered all local times at subauroral latitudes. Based on this campaign, we report two unique features at the beginning of the CIR storm of 21 March 2017: postmidnight tall purple auroral rays and global Pc1 geomagnetic pulsations over 13-hr local times from midnight to the afternoon sectors. Purple auroras are known to appear during or after very active auroras (IUGG, 1963), whereas the present event occurred during the quiet time before substorm/storm activity. We suggest that the tall purple auroral rays in the postmidnight sector were caused by the entry of high-density solar wind plasma from the magnetotail flank into the near-Earth plasma sheet, creating low-energy large-flux electron precipitation in the postmidnight sunlit ionosphere during the period of *calm before the storm*. The resonant scattering of sunlight by the molecular nitrogen ions can cause purple auroras at high altitudes. The repeated eastward (sunward) motion of the purple auroral rays also suggests that the source of this aurora is in the sunward convecting near-Earth plasma sheet.

Pc1 pulsations over a 13-hr MLT interval were observed by the unique PWING longitudinal network. We suggest that the entry of high-density solar wind plasma into the near-Earth plasma sheet under northward IMF conditions and the compression of the magnetosphere due to the solar wind density enhancement may create another population of high-energy ions in the plasma sheet through betatron acceleration and subsequently generate EMIC waves through temperature anisotropy. The dawnside appearance of the Pc1/EMIC waves of the present event also indicates that they were not caused by duskward drifting ions injected from the nightside magnetotail. The Arase XEP high-energy electron fluxes and model calculations of electron scattering rate by these waves show that these Pc1/EMIC waves may contribute to the loss of radiation belt particles observed by Arase at $L > 5.3$.

These results indicate interesting preconditioning of the magnetosphere due to high-density solar wind at the beginning of the CIR storm. This preconditioning with high-density solar wind will contribute to the creation of unique features of CIR storms compared with CME storms. The present results also indicate that the conjugate observation of the PWING ground network with Arase is a powerful tool to investigate wave and particle processes in the inner magnetosphere on a global scale.

Acknowledgments
The OMNI database was provided by https://omniweb.gsfc.nasa.gov/ow.html. The Arase XEP data processing was partly supported by the SEES/JAXA. Science data of the ERG (Arase) satellite were obtained from the ERG Science Center operated by ISAS/JAXA and ISEE/Nagoya University (http://ergsc.isee.nagoya-u.ac.jp/). The Arase satellite data will be publicly available via ERG Science Center on a project-agreed schedule. Support for the MACCS magnetometer data is provided by grant AGS-1651263 from the U.S. National Science Foundation. The present study analyzed fluxgate magnetometer v02.01 data generated on 28 July 2018. The present study analyzed XEP v001 data generated on 6 January 2018 and 8 August 2017 for 20 and 21 March 2017 data, respectively. This work is supported by the JSPS KAKENHI (15H05747, 15H05815, and 16H06286). This work is supported by the Ministry of Science and Higher Education of the Russian Federation and the Siberian Branch of the Russian Academy of Sciences (Project II.16.2.1, registration number AAAA-A17-117021450059-3; DGB). Observations at HUS were carried out under an agreement of cooperation between the Science Institute, University of Iceland (SIUI), and National Institute of Polar Research, Japan. Special thanks are due to Gunnlaugur Bjornsson in SIUI. The database construction for the PWING ground-based instruments is supported by the ERG Science Center (http://ergsc.isee.nagoya-u.ac.jp/) and the IUGONET (Inter-university Upper atmosphere Global Observation NETwork) project (http://www.iugonet.org/).

References

Arnoldy, R. L., Engebretson, M. J., Denton, R. E., Posch, J. L., Lessard, M. R., Maynard, N. C., et al. (2005). Pc 1 waves and associated unstable distributions of magnetospheric protons observed during a solar wind pressure pulse. *Journal of Geophysical Research*, *110*, A07229. https://doi.org/10.1029/2005JA011041

Borovsky, J. E., & Denton, M. H. (2006). Differences between CME-driven storms and CIR-driven storms. *Journal of Geophysical Research*, *111*, A07S08. https://doi.org/10.1029/2005JA011447

Borovsky, J. E., & Steinberg, J. T. (2006). The "calm before the storm" in CIR/magnetosphere interactions: Occurrence statistics, solar wind statistics, and magnetospheric preconditioning. *Journal of Geophysical Research*, *111*, A07S10. https://doi.org/10.1029/2005JA011397

Borovsky, J. E., Thomsen, M. F., & Elphic, R. C. (1998). The driving of the plasma sheet by the solar wind. *Journal of Geophysical Research*, *103*(A8), 17,617–17,639. https://doi.org/10.1029/97JA02986

Engebretson, M. J., Hughes, W. J., Alford, J. L., Zesta, E., Cahill, L. J. Jr., Arnoldy, R. L., & Reeves, G. D. (1995). Magnetometer array for cusp and cleft studies observations of the spatial extent of broadband ULF magnetic pulsations at cusp/cleft latitudes. *Journal of Geophysical Research*, *100*(A10), 19,371–19,386. https://doi.org/10.1029/95JA00768

Engebretson, M. J., Peterson, W. K., Posch, J. L., Klatt, M. R., Anderson, B. J., Russell, C. T., et al. (2002). Observations of two types of Pc 1–2 pulsations in the outer dayside magnetosphere. *Journal of Geophysical Research*, *107*(A12), 1451. https://doi.org/10.1029/2001JA000198

Engebretson, M. J., Posch, J. L., Wygant, J. R., Kletzing, C. A., Lessard, M. R., Huang, C. L., et al. (2015). Van Allen probes, NOAA, GOES, and ground observations of an intense EMIC wave event extending over 12 h in magnetic local time. *Journal of Geophysical Research: Space Physics*, *120*, 5465–5488. https://doi.org/10.1002/2015JA021227

Fraser, B. J., Grew, R. S., Morley, S. K., Green, J. C., Singer, H. J., Loto'aniu, T. M., & Thomsen, M. F. (2010). Storm time observations of electromagnetic ion cyclotron waves at geosynchronous orbit: GOES results. *Journal of Geophysical Research*, *115*, A05208. https://doi.org/10.1029/2009JA014516

Fujita, S., & Tamao, T. (1988). Duct propagation of hydromagnetic waves in the upper ionosphere, 1. Electromagnetic field disturbances in high latitudes associated with localized incidence of a shear Alfvén wave. *Journal of Geophysical Research*, *93*(A12), 14,665–14,673. https://doi.org/10.1029/JA093iA12p14665

Greifinger, P. (1972). Micropulsations from a finite source. *Journal of Geophysical Research*, *77*(13), 2392–2396. https://doi.org/10.1029/JA077i013p02392

Higashio, N., Takashima, T., Shinohara, I., & Matsumoto, H. (2018). The extremely high-energy electron experiments (XEP) onboard the Arase satellite. *Earth, Planets and Space*, *70*(1). https://doi.org/10.1186/s40623-018-0901-x

Hunten, D. M. (2003). Sunlit aurora and the N_2^+ ion: A personal perspective. *Planetary and Space Science*, *51*(13), 887–890. https://doi.org/10.1016/S0032-0633(03)00079-5

Hyun, K., Kim, K.-H., Lee, E., Kwon, H.-J., Lee, D.-H., & Jin, H. (2014). Loss of geosynchronous relativistic electrons by EMIC wave scattering under quiet geomagnetic conditions. *Journal of Geophysical Research: Space Physics*, *119*, 8357–8371. https://doi.org/10.1002/2014JA020234

Iles, R. H. A., Fazakerley, A. N., Johnstone, A. D., Meredith, N. P., & Bühler, P. (2002). The relativistic electron response in the outer radiation belt during magnetic storms. *Annales de Geophysique*, *20*(7), 957–965. https://doi.org/10.5194/angeo-20-957-2002

International Union of Geodesy and Geophysics (IUGG) (1963). *International Auroral Atlas*. Edinburgh: Edinburgh University Press.

Jordanova, V. K., Albert, J., & Miyoshi, Y. (2008). Relativistic electron precipitation by EMIC waves from self-consistent global simulations. *Journal of Geophysical Research*, *113*, A00A10. https://doi.org/10.1029/2008JA013239

Kataoka, R., & Miyoshi, Y. (2006). Flux enhancement of radiation belt electrons during geomagnetic storms driven by coronal mass ejections and corotating interaction regions. *Space Weather*, *4*, S09004. https://doi.org/10.1029/2005SW000211

Kim, K.-H., Omura, Y., Jin, H., & Hwang, J. (2017). A case study of EMIC waves associated with sudden geosynchronous magnetic field changes. *Journal of Geophysical Research: Space Physics*, *122*, 3322–3341. https://doi.org/10.1002/2016JA023391

Kumamoto, A., Tsuchiya, F., Kasahara, Y., Kasaba, Y., Kojima, H., Yagitani, S., et al. (2018). High Frequency Analyzer (HFA) of Plasma Wave Experiment (PWE) onboard the Arase spacecraft. *Earth, Planets and Space*, *70*(1). https://doi.org/10.1186/s40623-018-0854-0

Matsuoka, A., Teramoto, M., Nomura, R., Nose, M., Fujimoto, A., Tanaka, Y., et al. (2018). The ARASE (ERG) magnetic field investigation. *Earth, Planets and Space*, https://doi.org/10.1186/s40623-018-0800-1, *70*(1).

Miyoshi, Y., & Kataoka, R. (2005). Ring current ions and radiation belt electrons during geomagnetic storms driven by coronal mass ejections and corotating interaction regions. *Geophysical Research Letters*, *32*, L21105. https://doi.org/10.1029/2005GL024590

Miyoshi, Y., & Kataoka, R. (2008). Flux enhancement of the outer radiation belt electrons after the arrival of stream interaction regions. *Journal of Geophysical Research*, *113*, A03S09. https://doi.org/10.1029/2007JA012506

Miyoshi, Y., Kataoka, R., Kasahara, Y., Kumamoto, A., Nagai, T., & Thomsen, M. F. (2013). High-speed solar wind with southward interplanetary magnetic field causes relativistic electron flux enhancement of the outer radiation belt via enhanced condition of whistler waves. *Geophysical Research Letters*, *40*, 4520–4525. https://doi.org/10.1002/grl.50916

Miyoshi, Y., Sakaguchi, K., Shiokawa, K., Evans, D., Albert, J., Connors, M., & Jordanova, V. (2008). Precipitation of radiation belt electrons by EMIC waves, observed from ground and space. *Geophysical Research Letters*, *35*, L23101. https://doi.org/10.1029/2008GL035727

Miyoshi, Y., Shinohara, I., Takashima, T., Asamura, K., Higashio, N., Mitani, T., et al. (2018). Geospace Exploration Project ERG. *Earth, Planets and Space*, *70*(1). https://doi.org/10.1186/s40623-018-0862-0

Olson, J. V., & Lee, L. C. (1983). Pc1 wave generation by sudden impulses. *Planetary and Space Science*, *31*(3), 295–302. https://doi.org/10.1016/0032-0633(83)90079-X

Olson, W. P., & Pfitzer, K. A. (1977). Magnetospheric magnetic field modeling, Annual Scientific Report, AFOSR Contract No. F44620–75-C-0033.

Omura, Y., & Zhao, Q. (2012). Nonlinear pitch angle scattering of relativistic electrons by EMIC waves in the inner magnetosphere. *Journal of Geophysical Research*, *117*, A08227. https://doi.org/10.1029/2012JA017943

Park, J.-S., Kim, K.-H., Shiokawa, K., Lee, D.-H., Lee, E., Kwon, H.-J., et al. (2016). EMIC waves observed at geosynchronous orbit under quiet geomagnetic conditions ($Kp \leq 1$). *Journal of Geophysical Research: Space Physics*, *121*, 1377–1390. https://doi.org/10.1002/2015JA021968

Sandanger, M. I., Søraas, F., Sørbø, M., Aarsnes, K., Oksavik, K., & Evans, D. S. (2009). Relativistic electron losses related to EMIC waves during CIR and CME storms. *Journal of Atmospheric and Solar - Terrestrial Physics*, *71*(10-11), 1126–1144. https://doi.org/10.1016/j.jastp.2008.07.006

Shiokawa, K., Katoh, Y., Hamaguchi, Y., Yamamoto, Y., Adachi, T., Ozaki, M., et al. (2017). Ground-based instruments of the PWING project to investigate dynamics of the inner magnetosphere at subauroral latitudes as a part of the ERG-ground coordinated observation network. *Earth, Planets and Space*, *69*(1), 160. https://doi.org/10.1186/s40623-017-0745-9

Shiokawa, K., Nomura, R., Sakaguchi, K., Otsuka, Y., Hamaguchi, Y., Satoh, M., et al. (2010). The STEL induction magnetometer network for observation of high-frequency geomagnetic pulsations. *Earth, Planets and Space*, *62*(6), 517–524. https://doi.org/10.5047/eps.2010.05.003

Summers, D., & Thorne, R. M. (2003). Relativistic electron pitch-angle scattering by electromagnetic ion cyclotron waves during geomagnetic storms. *Journal of Geophysical Research*, *108*(A4), 1143. https://doi.org/10.1029/2002JA009489

Terasawa, T., Fujimoto, M., Mukai, T., Shinohara, I., Saito, Y., Yamamoto, T., et al. (1997). Solar wind control of density and temperature in the near-Earth plasma sheet: WIND/GEOTAIL collaboration. *Geophysical Research Letters*, *24*, 935–938. https://doi.org/10.1029/96GL04018

Tsurutani, B. T. (2001). The interplanetary causes of magnetic storms, substorms and geomagnetic quiet. In I. A. Daglis (Ed.), *Space storms and space weather hazards* (pp. 103–130). Dordrecht: Kluwer.

Tsurutani, B. T., Gonzalez, W. D., Gonzalez, A. L. C., Tang, F., Arballo, J. K., & Okada, M. (1995). Interplanetary origin of geomagnetic activity in the declining phase of the solar cycle. *Journal of Geophysical Research*, *100*(A11), 21,717–21,733. https://doi.org/10.1029/95JA01476

Tsurutani, B. T., Gonzalez, W. D., Gonzalez, A. L. C., Guarnieri, F. L., Gopalswamy, N., Grande, M., et al. (2006). Corotating solar wind streams and recurrent geomagnetic activity: A review. *Journal of Geophysical Research*, *111*, A07S01. https://doi.org/10.1029/2005JA011273

Usanova, M. E., Mann, I. R., Rae, I. J., Kale, Z. C., Angelopoulos, V., Bonnell, J. W., et al. (2008). Multipoint observations of magnetospheric compression-related EMIC Pc1 waves by THEMIS and CARISMA. *Geophysical Research Letters*, *35*, L17S25. https://doi.org/10.1029/2008GL034458

Zhou, X.-Y., & Smith, E. J. (2015). Supercriticality of ICME and CIR shocks. *Journal of Geophysical Research: Space Physics*, *120*, 1526–1536. https://doi.org/10.1002/2014JA020700